



Received: 27/10/2021

Accepted: 06/11/2021

Anales de Edificación

Vol. 8, Nº1, 46-52 (2022)

ISSN: 2444-1309

Doi: 10.20868/ade.2022.5022

## Comportamiento de las bandas de rotura de puente térmico en tabiques ligeros con entramado de acero Performance of thermal break strips in lightweight steel framed partition walls

Paulo Santos<sup>a</sup>; David Abrantes<sup>a</sup>; Paulo Lopes<sup>a</sup>; Diogo Mateus<sup>a</sup>

<sup>a</sup> ISISE, Department of Civil Engineering, University of Coimbra, Coimbra, Portugal

**Resumen**— En este trabajo, se midió la resistencia térmica global superficie-superficie (valor R) de diez configuraciones diferentes de tabiques interiores LSF en condiciones controladas de laboratorio. Las pruebas de laboratorio se llevaron a cabo utilizando un aparato de caja mini caliente con un conjunto de dos cámaras climáticas, siendo el rendimiento térmico de las paredes LSF medido utilizando el método de medidor de flujo de calor. Los resultados experimentales se compararon con simulaciones numéricas de elementos finitos. Se evaluaron tres materiales de tiras de rotura de puente térmico (TB) y tres ubicaciones de TB y se compararon con el rendimiento térmico de una pared de referencia sin tiras de TB. En cuanto a los materiales de las bandas de rotura de puente térmico, se llegó a la conclusión de que el mejor rendimiento térmico se obtiene con el aerogel. En cuanto a la ubicación de las tiras TB, la aplicación en el lado interior o exterior presenta rendimientos muy similares y la aplicación en ambos lados del montante de acero muestra un aumento significativo relativo del rendimiento térmico. El espesor de las tiras de TB también tiene una influencia significativa en la resistencia térmica de la pared.

**Palabras clave**— Rendimiento térmico; Bandas de rotura de puente térmico; Estructura ligera de acero; Tabiques divisorios; Mediciones.

**Abstract**— In this paper, the overall surface-to-surface thermal resistance (R-value) of ten different configurations from interior partition LSF walls were measured under controlled laboratory conditions. The laboratorial tests were performed using a mini hot box apparatus with a set of two climatic chambers, being the thermal performance of LSF walls measured using the heat flux meter method. The experimental results were compared with finite element numerical simulations. Three Thermal Break (TB) strips materials and three TB locations are assessed and compared with the thermal performance of a reference wall without TB strips. Regarding the TB strips materials, it was concluded that the best thermal performance is achieved by aerogel. Considering the TB strips location, the application inner or outer side, presents very similar performances and the application on both sides of steel stud shows a relative significant thermal performance increase. The thickness of the TB strips also has a significant influence on the wall thermal resistance.

**Index Terms**— Thermal performance; Thermal break strips; Lightweight steel frame; Partition walls; Measurements.

### I. INTRODUCTION

Energy efficiency and thermal comfort in buildings are mostly influenced by the characteristics of the envelope. Regarding lightweight steel framed (LSF) walls, the high thermal conductivity of steel can lead to significant thermal bridges, which must be predicted at building design phase and treated at construction stage (Ribeiro et al., 2021).

A usual LSF wall is mainly composed of three parts: (1) steel frame internal structure (cold form studs); (2) sheathing panels (internal and external, e.g., gypsum plasterboard and OSB – Oriented Strand Board); (3) the insulation layers (cavity/batt insulation, such as mineral wool, and/or ETICS - Exterior

Thermal Insulation Composite System) (Santos, 2017). The batt insulation, besides the thermal insulation function, can also perform as an important acoustic insulation (Roque et al., 2019). The effectiveness of thermal insulation depends on its position in the LSF element, as well on the type of LSF construction (Roque et al., 2017; Santos et al., 2019). In fact, the existence of an insulation layer and its position on the wall determines the type of LSF construction. According to Santos et al. (2012), an LSF construction can be classified into three walls frame typologies: (1) cold, (2) hybrid and (3) warm. On cold frame constructions, all the thermal insulation is placed inside the air cavity, between the vertical studs and limited to

the stud deep. On warm frame construction, all insulation is continuous and located outside of the steel frame (ETICS). Given its advantages, the hybrid construction type is used more often, it's an intermediate solution between cold and warm construction and has both types of insulation applied (Roque et al., 2019).

There are three main approaches to obtain thermal resistance/transmittance of building elements: (1) analytical, (2) numerical, and (3) measurements (Santos et al., 2019). The use of analytical formulas could be the simplest approach of all three methods, being very useful and easy to use by designers (Gorgolewski et al., 2007). However, this analytical approach is usually only available for simpler configurations, its application being most often, very limited. Moreover, these formulations frequently consider a simplified steady-state one-dimensional (1D) heat transfer and do not consider the heat storage inside the material, or the thermal properties variation (e.g., with temperature and humidity)(ASHRAE, 2017). Numerical simulations could be performed with two-dimensional (2D) models, or three-dimensional (3D) models (Roque et al., 2017; Santos et al., 2019; Martins et al., 2016; Santos et al., 2014). They have the advantage of allowing a quick comparison between several building component solutions/configurations. However, they need a specific software tool. To ensure the reality of the obtained results the models should be validated with measurements or at least verified by comparison with benchmark results. Regarding thermal performance measurements, they could be accomplished in-situ or in laboratory settings, being crucial for the validation of numerical and analytical methods (Soares et al., 2019). There are various measurement methods, the most used ones being: the Heat Flow Meter (HFM); the Guarded Hot Plate (GHP); the Hot Box (HB), which could be Calibrated (CHB) or Guarded (GHB); and InfraRed Thermography (IRT) (Soares et al., 2019).

Nowadays, several techniques could be used to mitigate thermal bridges in LSF building elements, such as slotted thermal steel studs (Martins et al.; Lupan et al., 2016; Váradi et al., 2009), Thermal Break (TB) strips (Santos et al., 2019; Váradi et al., 2009; Santos et al., 2020), continuous thermal insulation layers (e.g., ETICS) (Santos et al., 2019; Kapoor et al.; Kempton et al., 2021). Moreover, when there is a cavity inside the wall, one effective way to improve the thermal performance is by reducing the heat transfer by radiation. This could be achieved by using reflective low-emissivity paint or foil inside the air gaps of the building elements (Santos et al.; Bruno et al., 2021; Jelle et al., 2015).

In this work, with the intention of evaluating the TB strips performance for the mitigation of thermal bridges, originated by the high thermal conductivity of steel studs, the overall surface-to-surface thermal resistance (R-value) of ten different configurations of LSF partition walls were measured under controlled laboratory conditions. These laboratorial tests were performed using a mini hot box apparatus with a set of two climatic chambers (cold and hot), being the thermal performance of LSF walls measured using the Heat Flux Meter

(HFM) method (ISO9869-1, 2014). For each wall, three tests were performed, applying the sensors at top, middle and bottom, within the LSF wall test-sample surfaces, totaling thirty lab tests. The TB strips materials tested were aerogel, recycled rubber-cork composite, and pine wood. Three different configurations for the localization of the TB strips were considered, along the: inner, outer and both steel flanges. Furthermore, to perform a verification of the experimental values, all the LSF walls measurements results (overall conductive R-values) were compared with 2D and 3D finite element numerical simulations computed through the software THERM® and ANSYS®, respectively.

## II. MATERIALS AND METHODS

### A. LSF partition wall description

In this section the characterization regarding materials, geometry, dimensions, and thermal properties of the LSF reference wall and the thermal break (TB) strips is accomplished. The reference LSF Wall is a configuration of a wall normally used as an internal partition within the same house. As illustrated in Figure 1 the total thickness of the reference LSF partition wall is 140 mm, where the outer and inner sheathing surfaces are constituted by two Gypsum Plaster Boards (GPB) (12.5 mm thick) on each side of vertical steel studs (C90 x 37 x 5 x 0.6 mm) spaced 400 mm apart, and the air cavity is entirely filled with Mineral Wool (MW) batt insulation (90 mm thick). In Table 1 is presented the thickness and thermal conductivities values of the LSF partition wall materials.

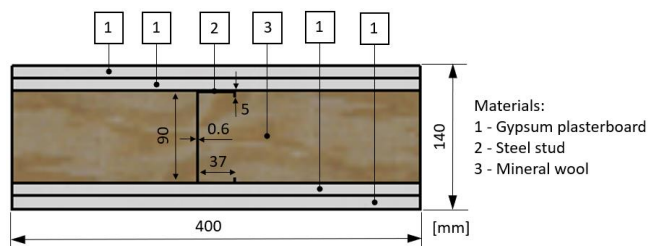


Fig. 1. Horizontal cross-section of the reference LSF partition wall: geometry, dimensions, and materials

TABLE I  
REFERENCE LSF PARTITION WALL MATERIAL THICKNESS (D) AND THERMAL CONDUCTIVITIES ( $\lambda$ ) VALUES OF THE LSF PARTITION WALL MATERIALS

Material	$d$ [mm]	$\lambda$ [W/(m·K)]
GPB1 (2 x 12.5 mm)	25	0.175
MW2	90	0.035
Steel Stud (C90 x 37 x 5 x 0.6 mm)	---	50.000
GPB1 (2 x 12.5 mm)	25	0.175
<b>Total Thickness</b>	140	---

The TB strips analysed are 50 mm wide and 10 mm thick. Figure 2 illustrates the materials used, namely Pine Wood (PW), recycled rubber and cork composite (MS-R0), and aerogel (AG). Notice that the thickness of PW strips is slightly higher (13 mm), than the nominal thickness (10 mm). In Table 2 are displayed the thermal conductivities of these TB strip materials, ranging from 0.130 W/(m·K) for PW, down to 0.015 W/(m·K) for AG. As illustrated in Figure 3 the TB strips will be placed in three different configuration positions, along the inner, outer and on both steel stud flanges.



(a) Pine Wood (PW) (b) Rubber-Cork (MS-R0) (c) Aerogel (AG)  
Fig. 2. Thermal break strips materials used on the LSF partition walls

TABLE I  
THERMAL BREAK STRIPS: MATERIALS AND THERMAL CONDUCTIVITY ( $\lambda$ )

Material	$\lambda$ [W/(m·K)]	Ref.
Pine Wood (PW)	0.130	(Santos, 2006)
Rubber-Cork Composite (MS-R0)	0.088	(MS-R0, 2008)
CBS1 Aerogel (AG)	0.015	(Proctor Group, 2018)

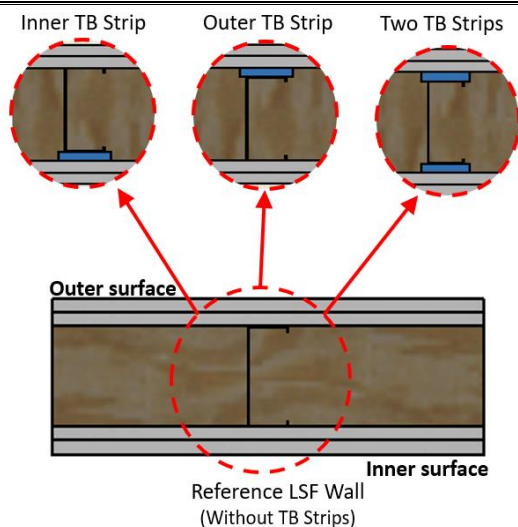


Fig. 3. Geometry and location of the Thermal Break (TB) strips

**B. Experimental lab Measurements**

The laboratorial tests were performed using a mini hot box apparatus, where the wall sample is set between two climatic chambers (cold box and hot box), as illustrated in Figure 4(a). Notice that the wall sample perimeter was covered by 80 mm

of polyurethane foam insulation (not illustrated) having a thermal conductivity of 0.036 W/(m·K), to mitigate the heat losses through the LSF wall perimeter. The cold box is cooled by a refrigerator, while the hot box is heated by an electrical resistance (70 watts). The wall samples used in the tests have 1060 mm wide and 1030 mm high, with a structure composed of three vertical steel studs, spaced 400 mm, where the middle one is centred. The thermal performance of the LSF walls was obtained using the Heat Flux Meter (HFM) method (ISO9869-1, 2014), adapted for two HFM sensors, one in each wall surface (Soares et al., 2019). Four Hukseflux sensors (model HFP01), with a precision of  $\pm 3\%$ , were used to measure the heat flux through the LSF wall, two on the hot surface and the other two on the cold surface, increasing the accuracy of the measurements and reducing the duration of the test, as suggested by Rasooli and Itard (Rasooli et al., 2018). In both surfaces (hot and cold) one HFM was placed over the middle vertical steel stud and another one in the middle of the insulation cavity, as illustrated in Figure 4(b), to measure two distinct thermal behaviour zones.

The temperature measurements were obtained using twelve Type K (1/0.315) PFA insulated ThermoCouples (TCs), certified with a class 1 precision. Half of them were used on the hot side and the other half on the cold side. Moreover, two TCs measured the environment air temperature inside both chambers (hot and cold), another two TCs measured the temperatures of the wall surface near the HFMs and the remaining two measured the air temperature near the wall surface, as illustrated in Figure 4(b) for the cold wall surface.

The cold and hot chambers were set to maintain a temperature of 5°C and 40°C, respectively. These two climatic chambers were well insulated to minimize surrounding heat losses and to ensure that the measurements were made in a quasi-steady-state heat transfer condition.

The temperatures and heat flux measured during the tests were recorded using one Pico TC-08® data-logger, with a precision of  $\pm 0.5^\circ\text{C}$ , on each side of the LSF wall. This data was managed by the software PicoLog® (version 6.1.10) in a computer connected to the data-loggers.

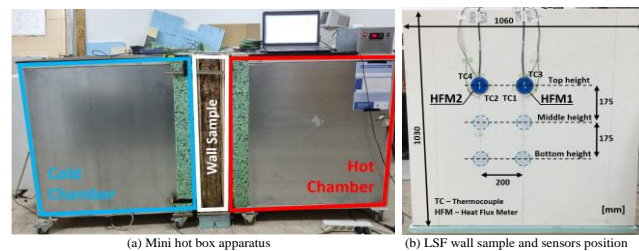


Fig. 4. Experimental lab tests illustrations.

**C. Numerical simulations**

The thermal bidimensional numerical simulations of the LSF walls were accomplished using the software THERM® (version 7.6.1), based on Finite Element Method (FEM). These simulations only consider a 2D representative part of the walls cross-section (400 mm wide), as previously illustrated in Figure 1 for the reference LSF partition wall. In these simulations the thermal properties for the different materials were presented in

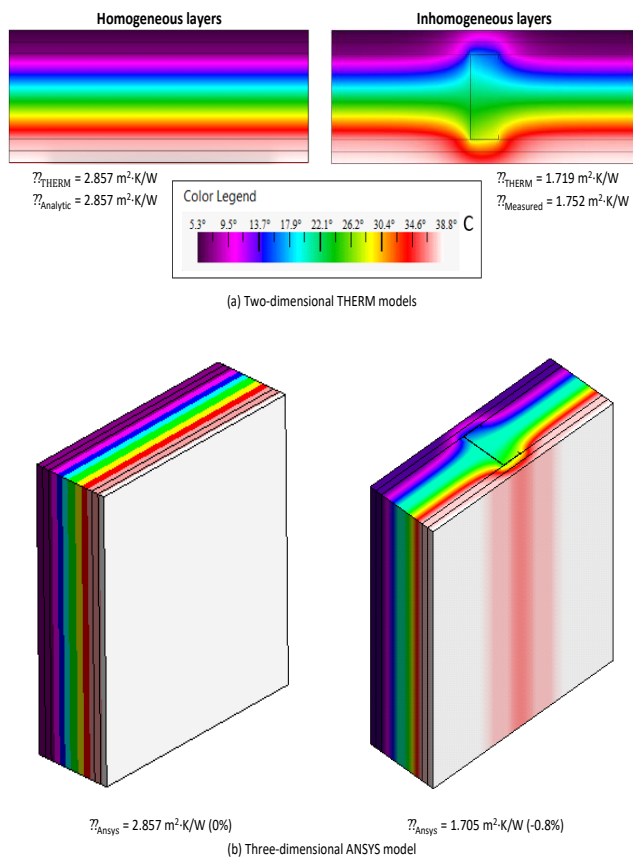


Fig. 5. Accuracy verification of the THERM models: Temperature distribution and conductive R-values.

Table 1 and Table 2. Furthermore, the maximum error accepted on the FEM computations was set to 2%, for all models built and assessed in this work.

Two sets of boundary conditions were defined for each simulation, by defining two parameters, which were the environment air temperature and the surface film coefficient. The air temperature for the cold and hot environment were set to the temperature values, defined for the cold and hot chambers in lab measurements, i.e., 5°C and 40°C, respectively. The surface film coefficients were modelled using the average values measured in each test and for each LSF wall surface, considering the difference between air and surface temperatures, and the surface heat fluxes. The surface thermal resistances ranged within the interval defined in ISO 6946 (ISO-6946, 2017) for horizontal heat flow (0.04-0.13 m·K/W).

The accuracy of the THERM®, 2D models, was also verified by comparison with 3D models, created in ANSYS® WORKBENCH software (version 19.1). Notice that the boundary conditions used in these simulations are in accordance with the laboratory measurements. Figure 5 displays the coloured temperature distribution for the reference partition wall model build in: (a) THERM, and (b) ANSYS. As illustrated, both simulated coloured temperature distributions of the LSF partition wall are analogous. Furthermore, the obtained surface-to-surface thermal resistances (R-values) are very similar, having a nearly zero difference (i.e., 0.8%).

### III. RESULTS Y DISCUSSION

#### A. Conductive thermal resistances

In Table 3 are displayed the laboratory measurements and the values predicted by 2D FEM models using the software THERM for the conductive thermal resistances of the studied LSF partition walls, as well as the differences between them in percentage and absolute values. The results are divided in four groups: (1) the reference LSF partition wall (Ref.); (2) the LSF partition walls with an inner TB strip (PWin, R0in and AGin); (3) the LSF partition walls with an outer TB strip (PWout, R0out and AGout); and (4) the LSF partition walls with a TB strip on both sides, inner and outer (PWx2, R0x2 and AGx2).

The measured R-values and the predicted ones are quite similar, being the biggest differences in percentages of ±2%. Thus, ensuring the reliability of both measured and predicted R-values. Thermal Break (TB) strips mitigates the heat losses due to the steel stud thermal bridges, increasing the thermal resistance of the LSF partition walls. This increase depends mainly on the number of TB strips, its material thermal conductivity and their thickness.

In Figure 6 the measured R-values are graphically displayed, for an easier visualization and comparison. Since the MW batt insulation is expansible, it is also displayed the R-value rise duo to a homogeneous MW layer increment of 10 and 20 mm, equivalent to thickness of one and two TB strips, respectively.

TABLE III  
THERMAL BREAK STRIPS: MATERIALS AND THERMAL CONDUCTIVITY ( $\Delta$ )

Wall Code Wall Description	R-value		Difference	
	THERM (m <sup>2</sup> ·K)/W	Tested (m <sup>2</sup> ·K)/W	Abs. (m <sup>2</sup> ·K)/W	Perc. [%]
<b>Ref.</b>				
<b>Reference LSF Partition Wall</b>	1.719	1.752	+0.033	+2%
<b>PWin</b>				
<b>Inner Pine Wood TB Strip</b>	1.976	1.931	-0.045	-2%
<b>R0in</b>				
<b>Inner Rubber-Cork TB Strip</b>	2.006	2.006	+0.000	0%
<b>AGin</b>				
<b>Inner Aerogel TB Strip</b>	2.359	2.404	+0.045	+2%
<b>PWout</b>				
<b>Outer Pine Wood TB Strip</b>	1.981	1.976	-0.005	0%
<b>R0out</b>				
<b>Outer Rubber-Cork TB Strip</b>	1.975	1.965	-0.010	-1%
<b>AGout</b>				
<b>Outer Aerogel TB Strip</b>	2.358	2.414	+0.056	+2%
<b>PWx2</b>				
<b>Double Pine Wood TB Strips</b>	2.254	2.304	+0.050	+2%
<b>R0x2</b>				
<b>Double Rubber-Cork TB Strips</b>	2.236	2.202	-0.034	-2%
<b>AGx2</b>				
<b>Double Aerogel TB Strips</b>	2.892	2.885	-0.007	0%

The thermal conductivity of MW batt insulation (0.035 W/m·K) is lower than R0 composite (0.088 W/m·K) and PW (0.130 W/m·K), being higher in relation to AG (0.015 W/m·K). So, as expected, when using TB materials with lower thermal conductivities, the thermal performance improvement is lower than the one expected for a homogeneous MW layer. This R-value increase for a single TB strip ranges from +10% up to +14% and for double TB strips from +26% to +32%. However, the R-values for the LSF partition walls with aerogel TB strips are higher than the expected ones for the homogeneous MW increased layer, being the thermal performance enhance for these TB strips equal to +37% (inner); +38% (outer), and +65% (double TB strips).

Notice that the configuration of the aerogel TB strips on both sides of the steel stud presents a conductive thermal resistance of 2.885 m<sup>2</sup>·K/W, which means that it fully mitigates the steel frame thermal bridges effect, since it reaches the R-value for a homogeneous wall without steel studs, which is 2.857 m<sup>2</sup>·K/W, as graphically displayed in Figure 6 as a vertical dashed line.

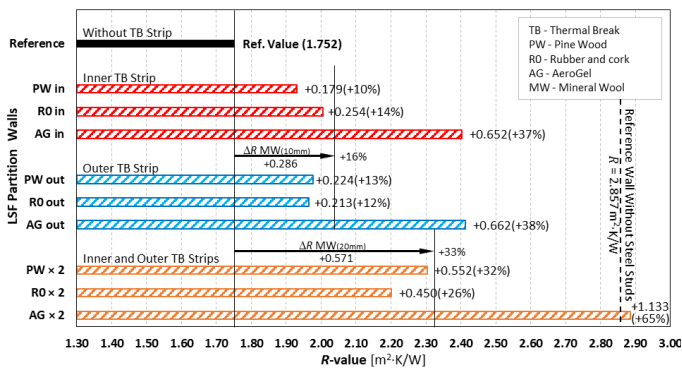


Fig. 6. Measured conductive thermal resistances of LSF partition walls.

Another interesting and quite surprising feature in Figure 6 is that for the TB strips on the outer flange and with TB strips on both sides of the steel studs, the R-values measured when using Pine Wood (PW) are higher than when using rubber-cork composite (R0), even when PW has an higher thermal conductivity (0.130 W/(m·K)). This happens since pine wood TB strips instead of having 10 mm thick, have 13 mm thick, which also originates a bigger MW expansion of 3 and 6 mm, for single and double TB strips, respectively.

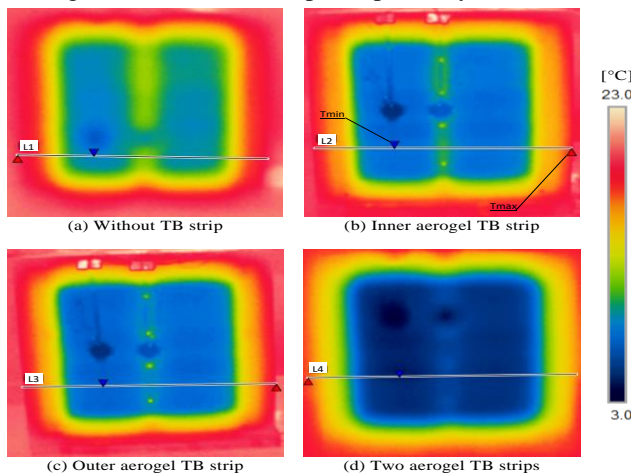


Fig. 7. IR images of the assessed LSF partition walls: Cold surface (Santos et al., 2020).

### B. Thermographic Images

In Figure 7 is illustrated the infrared (IR) images taken to the tested LSF partition walls on the cold surface, for the reference wall and for the LSF partition walls with aerogel TB strips, with the purpose of assessing the steel stud thermal bridge mitigation effect. Additionally, in Figure 8 is displayed the surface temperature profiles recorded along the lines (L1 to L4) identified in the Figure 7.

Looking at the IR images, can easily be detected in Figure 7(a) (LSF partition wall without TB strips) the vertical steel stud in the centre, due to the increased localized heat transfer, originating a higher surface temperature in the cold surface. In comparison, the central vertical steel stud in Figure 7(d) is the least pronounced, since the heat transfer for the LSF partition wall with aerogel TB strips on both sides of the steel studs is mitigated the most, reducing very significantly the related thermal bridge effect.

### C. Heat flux predictions

A similar assessment was performed using 2D FEM models, computed in THERM, as illustrated in Figure 8, where is displayed the predicted heat flux distribution along the cross-section of the four LSF partition walls previously presented in Figure 7.

In Figure 8(a), the higher heat flux is well visible along the section containing the steel stud, due to the thermal bridge effect. This increased heat flux is related to the higher heat conduction along the steel studs, well visible on both sides of the sheathing layers, mainly around the steel flanges, which diffuses heat to the gypsum plasterboards. Notice that in the web of the steel stud there is also a significant heat flux, which is not well visible in this scale. When there is an aerogel TB strip placed on the inner (Figure 9(b)) or outer (Figure 8(c)) steel flange, the heat flux through the steel flange has a significant decrease on the TB strip side. However, in all the remaining parts the reduction of the heat flux is not as pronounced.

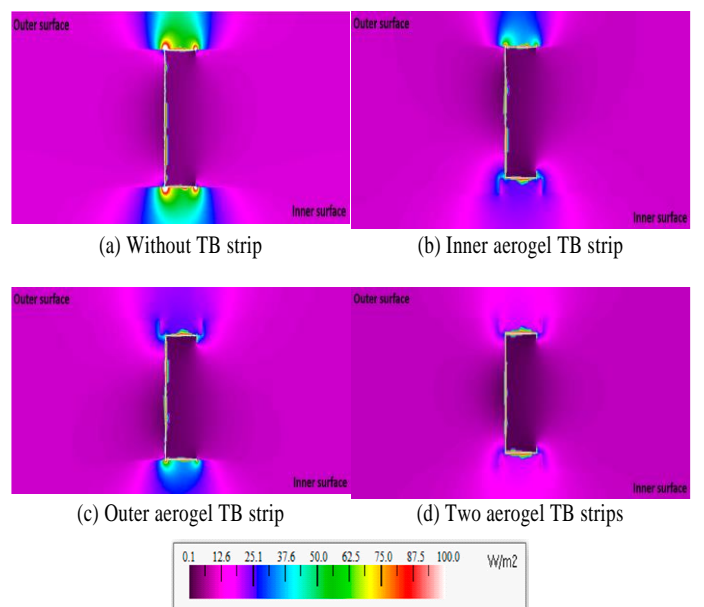


Fig. 8. Predicted heat flux distribution within the LSF walls cross-section.

Finally, in Figure 8(d) is illustrated the heat flux distribution when a TB strip is used on both steel stud flanges. As expected, the heat flux on both sides of these flanges is highly mitigated, leaving the major heat flux values mainly within the web steel stud. This last illustration allows to visualize how these two aerogel TB strips can fully mitigate the thermal bridges effect due to the steel studs.

#### IV. CONCLUSIONS

In this work the thermal performance of Lightweight Steel Framed (LSF) partition walls with Thermal Break (TB) strips were measured under controlled laboratory conditions. Three TB strips materials (Pine wood, Recycled rubber-cork composite and Aerogel) were tested. Moreover, three configurations regarding the location of the TB strips were considered (inner, outer and on both steel, stud flanges). For each of the configurations, three types of results were analysed: (1) the measured and numerically simulated conductive R-values, for all TB strips materials; (2) the recorded temperature at the cold surface through infrared images, using only aerogel TB strips, and (3) the THERM predicted heat flux for the same aerogel TB strip configurations.

The main conclusions of this research work could be summarized as follows:

As expected, the thermal performance achieved when a single TB strip is applied on inner or outer steel stud flanges is quite similar.

- The application of TB strips on both steel stud flanges provides a significant thermal resistance increase, compared to the application of a single TB strip and without any TB strip.
- Aerogel was the TB strip material with the best thermal performance, being this explained by its very reduced thermal conductivity, when compared with the remaining materials.
- The application of aerogel TB strips on both steel stud flanges was the only configuration able to fully mitigate the steel frame thermal bridge effect, reaching the R-value provided for the reference wall without steel studs.
- The thickness of the TB strips also has a significant influence on the wall thermal resistance, not only because it mitigates the local steel frame thermal bridge effect, but also due to the mineral wool expansion, which increases the thermal resistance along the cavity zone (between steel studs).

#### AGRADECIMIENTOS

This research was funded by FEDER funds through the Competitvity Factors Operational Programme – COMPETE and by national funds through FCT – Foundation for Science and Technology, within the scope of the project POCI-01-0145-FEDER 032061.

Financiado por: POCI-01-0145-FEDER-032061



#### REFERENCES

- ASHRAE. (2017). Handbook of Fundamentals (SI Edition). ASHRAE - American Society of Heating, Refrigerating and Air-conditioning Engineers, Atlanta, USA, 2017.
- Bruno, R., Bevilacqua, P., Ferraro, V., & Arcuri, N. (2021). Reflective thermal insulation in non-ventilated air-gaps: experimental and theoretical evaluations on the global heat transfer coefficient. *Energy and Buildings*, 236, 110769. <https://doi.org/10.1016/J.ENBUILD.2021.110769>
- Gorgolewski, M. (2007). Developing a simplified method of calculating U-values in light steel framing. *Building and Environment*, 42(1), 230–236. <https://doi.org/10.1016/j.buildenv.2006.07.001>
- Gyptec Ibérica. (2022). Technical Sheet: Standard Gypsum Plasterboard. [https://www.gyptec.eu/documentos/Ficha\\_Tecnica\\_Gyptec\\_A.pdf](https://www.gyptec.eu/documentos/Ficha_Tecnica_Gyptec_A.pdf)
- ISO 6946. (2017). Building components and building elements — Thermal resistance and thermal transmittance — Calculation methods, International Organization for Standardization.
- ISO 9869-1. (2014). Thermal insulation – Building elements - In-situ measurement of thermal resistance and thermal transmittance. Part 1: Heat flow meter method.
- Jelle, B. P., Kalnæs, S. E., & Gao, T. (2015). Low-emissivity materials for building applications: A state-of-the-art review and future research perspectives. *Energy and Buildings*, 96, 329–356. <https://doi.org/10.1016/J.ENBUILD.2015.03.024>
- Kapoor, D. R., & Peterman, K. D. (2021). Quantification and prediction of the thermal performance of cold-formed steel wall assemblies. *Structures*, 30, 305–315. <https://doi.org/10.1016/J.ISTRUC.2020.12.060>
- Kempton, L., Kokogiannakis, G., Green, A., & Cooper, P. (2021). Evaluation of thermal bridging mitigation techniques and impact of calculation methods for lightweight steel frame external wall systems. *Journal of Building Engineering*, 43, 102893. <https://doi.org/10.1016/J.JOBE.2021.102893>
- Lupan, L. M., Manea, D. L., & Moga, L. M. (2016). Improving Thermal Performance of the Wall Panels Using Slotted Steel Stud Framing. *Procedia Technology*, 22, 351–357. <https://doi.org/10.1016/J.PROTCY.2016.01.108>
- Martins, C., Santos, P., & da Silva, L. S. (2016). Lightweight steel-framed thermal bridges mitigation strategies: A parametric study. *Journal of Building Physics*, 39(4), 342–372. <https://doi.org/10.1177/1744259115572130>
- MS-R0 Test Report. (2008). Test report Ref. 5015 PE 1977/08 - Determination of Thermal Conductivity (Acousticork MS-R0). Departamento de Engenharia Têxtil, Universidade do Minho.
- Proctor Group. (2018). Spacetherm ® CBS Specification. <https://www.proctorgroup.com/assets/PerformanceSpecs/Spacetherm CBS Performance Specification.pdf>
- Rasooli, A., & Itard, L. (2018). In-situ characterization of walls' thermal resistance: An extension to the ISO 9869 standard

- method. *Energy and Buildings*, 179, 374–383. <https://doi.org/10.1016/j.enbuild.2018.09.004>
- Ribeiro, T., Santos, P., & Mateus, D. (2021). Performance of Thermal Break Strips in Lightweight Steel Framed Walls. In *Proceedings of the 1st International Conference on Water Energy Food and Sustainability (ICoWEFS 2021)* (pp. 382–389). Springer International Publishing. [https://doi.org/10.1007/978-3-030-75315-3\\_43](https://doi.org/10.1007/978-3-030-75315-3_43)
- Roque, E., & Santos, P. (2017). The effectiveness of thermal insulation in lightweight steel-framed walls with respect to its position. *Buildings*, 7(1). <https://doi.org/10.3390/buildings7010013>
- Roque, E., Santos, P., & Pereira, A. C. (2019). Thermal and sound insulation of lightweight steel-framed façade walls. *Science and Technology for the Built Environment*, 25(2), 156–176. <https://doi.org/10.1080/23744731.2018.1506677>
- Santos, C., & Matias, L. (2006). ITE50 - Coeficientes de Transmissão Térmica de Elementos da Envolvente dos Edifícios (in Portuguese). LNEC - Laboratório Nacional de Engenharia Civil.
- Santos, P. (n.d.). “Chapter 3 - Energy Efficiency of Lightweight Steel-Framed Buildings,” in *Energy Efficient Buildings*, Eng Hwa Yap, Ed. London, UK: InTech, 2017, pp. 35–60. <https://doi.org/10.5772/66136>
- Santos, P., Gonçalves, M., Martins, C., Soares, N., & Costa, J. J. (2019). Thermal transmittance of lightweight steel framed walls: Experimental versus numerical and analytical approaches. *Journal of Building Engineering*, 25. <https://doi.org/10.1016/j.jobe.2019.100776>
- Santos, P., Lemes, G., & Mateus, D. (2019). Thermal transmittance of internal partition and external facade LSF walls: A parametric study. *Energies*, 12(14). <https://doi.org/10.3390/en12142671>
- Santos, P., Martins, C., da Silva, L. S., & Bragança, L. (2014). Thermal performance of lightweight steel framed wall: The importance of flanking thermal losses. *Journal of Building Physics*, 38(1), 81–98. <https://doi.org/10.1177/1744259113499212>
- Santos, P., & Mateus, D. (2020). Experimental assessment of thermal break strips performance in load-bearing and non-load-bearing LSF walls. *Journal of Building Engineering*, 32, 101693. <https://doi.org/10.1016/j.jobe.2020.101693>
- Santos, P., & Ribeiro, T. (2021). Thermal performance improvement of double-pane lightweight steel framed walls using thermal break strips and reflective foils. *Energies*, 14(21). <https://doi.org/10.3390/en14216927>
- Santos, Paulo., Silva, L. S. da., & Ungureanu, V. (n.d.). *Energy Efficiency of Light-weight Steel-framed Buildings*, 1st ed. European Convention for Constructional Steelwork (ECCS), Technical Committee 14 - Sustainability & Eco-Efficiency of Steel Construction, ISBN 978-92-9147-105-8, N. 129, 2012.
- Soares, N., Martins, C., Gonçalves, M., Santos, P., da Silva, L. S., & Costa, J. J. (2019). Laboratory and in-situ non-destructive methods to evaluate the thermal transmittance and behavior of walls, windows, and construction elements with innovative materials: A review. In *Energy and Buildings* (Vol. 182, pp. 88–110). Elsevier Ltd. <https://doi.org/10.1016/j.enbuild.2018.10.021>
- Váradi, J., & Toth, E. (2009). Thermal Improvement of Lightweight Façades containing Slotted Steel Girders. In *Twelfth International Conference on Civil, Structural and Environmental Engineering Computing*.
- Volcalis. (2022). Technical Sheet: Alpha Mineral Wool. [https://www.volcalis.pt/categoria\\_file\\_docs/fichatecnica\\_volcalis\\_alpharollo-386.pdf](https://www.volcalis.pt/categoria_file_docs/fichatecnica_volcalis_alpharollo-386.pdf)



**Reconocimiento – NoComercial (by-nc):** Se permite la generación de obras derivadas siempre que no se haga un uso comercial. Tampoco se puede utilizar la obra original con finalidades comerciales.